High-Pressure Synthesis and Magnetic Properties of Layered Double Perovskites Ln_2CuMO_6 (Ln = La, Pr, Nd, and Sm; M = Sn and Zr)

Masaki Azuma,* Shingo Kaimori,† and Mikio Takano

Institute for Chemical Research, Kyoto University, Uji, Kyoto-fu 611, Japan

Received March 31, 1998. Revised Manuscript Received June 2, 1998

Ln_2CuSnO_6 (Ln = Pr, Nd, and Sm) and La_2CuZrO_6 have been stabilized in the same layered double perovskite structure as La_2CuSnO_6 at high pressures of 6−8 GPa. Their crystal structures and magnetic properties were investigated. Replacement of La^{3+} by smaller lanthanide ions and Sn^{4+} by larger Zr^{4+} increased the buckling of the Cu−O−Cu bonds in the CuO_2 layers. In Nd_2CuSnO_6, both the Cu and Nd sublattice were found to exhibit weak ferromagnetism owing to spin canting. The magnetization data showed an anomalous transition at 110 K.

Introduction

Since the discovery of the high-temperature superconductivity in $La_{2-x}Ba_xCuO_4$,[1] a large number of copper oxide superconductors have been found. Their common structural characteristic is the presence of two-dimensional CuO_2 sheets. Compounds with the general formula $(ABX_3)(AX)_n$ with $n = 0$, $^1/_3$, $^1/_2$, and 1 usually crystallize in a series of related structures with such 2D BX_2 sheets, so-called Ruddlesden−Popper phases[2,3] or layered perovskites. For example, $SrIrO_3$, $Sr_4Ir_3O_{10}$, $Sr_3Ir_2O_7$, and Sr_2IrO_4 represent the $n = 0-1$ phases, respectively.[4] It should be noted that only the last one is an ambient pressure phase, while the others are stabilized at high pressure. The situation is different for Cu^{2+} compounds. La_2CuO_4 is the only example of a layered perovskite phase without oxygen vacancies, and the other phases of this series, $SrCuO_2$,[5] $La_2Ca_2Cu_3O_8$,[6] and $La_2(Sr,Ca)Cu_2O_6$ [7] are oxygen deficient. Combined with tetravalent elements, however, it becomes possible to form the perovskite phases $LaCu_{1/2}M_{1/2}O_3$ (M = Mn, Ti, Ir, and Sn).[8] These phases are so-called double perovskites, and the configuration of the two B-cations depends on the ionic radius of the M^{4+} ion. In La_2CuTiO_6 the Cu^{2+} and Ti^{4+} ions are distributed randomly.[9] The Cu^{2+} and Ir^{4+} (or Mn^{4+}) ions are arranged in the rock-salt configuration.[10] La_2CuSnO_6 is the only double perovskite phase with a layered configuration of B-cations.[11] Despite the presence of the CuO_2 sheets, this material does not show superconductivity, even at an appreciable level of Sr or Ca substitution for La.[12] As shown in Figure 1, Cu−O−Cu bonds in the CuO_2 sheet of this material are heavily buckled, and thus the average bond length is close to 4 Å. This value is considerably larger than a typical value of 3.9 Å for superconductors with hole carriers. It was also shown that when doped with holes, the in-plane Cu−O−Cu bond length increased while that out-of-plane shrank. These results suggested that the conduction band in this compound was comprised of d_{z^2} orbitals rather than of $d_{x^2-y^2}$ as in other layered cuprates.

In this paper we report the replacement of La by smaller lanthanides in order to shrink the Cu−O−Cu bond length and possibly realize superconductivity in the doped compounds. Ln_2CuSnO_6 with smaller lanthanides, Pr, Nd, and Sm, were stabilized at high pressure, and their magnetic properties were examined. Stabilization of the layered double perovskite La_2CuMO_6 was also studied, and La_2CuZrO_6, a new example of the layered double perovskite with a larger tetravalent cation, was discovered.

Experimental Section

Sample Preparation. Stoichiometric amounts of Ln_2O_3 (Ln = La, Nd, and Sm), CuO and SnO_2 were mixed, pressed into pellets, and heated at 1000 °C for 4 days in air with intermediate regrindings every day. Mixtures of Pr_6O_{11}, CuO, SnO, and SnO_2 were chosen as starting reagents for the Pr_2CuSnO_6 sample. Almost a single phase sample of the double perovskite was obtained for Ln = La, while the others were

* To whom correspondence should be addressed.
† Present address: Osaka Research Laboratories, Sumitomo Electric Industries, Ltd., 1-1-3, Simaya, Konohana, Osaka, 554 Japan.

(1) Bednortz, J. G. K.; Müller, A. *Z. Phys.* **1986**, *B64*, 189.
(2) Ruddlesden, S. N.; Popper, P. *Acta Crystallogr.* **1957**, *10*, 10.
(3) Ruddledsen, S. N.; Popper, P. *Acta Crystallogr.* **1958**, *11*, 54.
(4) Kafalas, J. A.; Longo, J. M. *J. Solid State Chem.* **1972**, *4*, 55.
(5) Okada, H.; Takano, M.; Takeda, Y. *Physica* **1991**, *C166*, 111.
(6) Gulloy, A. M.; Scott, B. A.; Figat, R. A. *J. Solid State Chem.* **1994**, *113*, 54.
(7) Cava, R. J.; Batlogg, B.; van Dover: R. B.; Krajewski, J. J.; Waszczak, J. V.; Fleming, R. M.; Peck, W. F., Jr.; Rupp, L. W., Jr.; Marsh, P.; James, A. C. W. P.; Schneemeyer, L. F. *Nature* **1990**, *345*, 602.
(8) Anderson, M. T.; Greenwood, K. B.; Taylor, G. A.; Poeppelmeier, K. R. *Prog. Solid State Chem.* **1993**, *22*, 197.
(9) Ramadass, N.; Gopalakrishnan, J.; Sastri, M. V. C. *J. Inorg. Nucl. Chem.* **1978**, *40*, 1453.
(10) Blasse, G. *J. Inorg. Nucl. Chem.* **1965**, *27*, 993.
(11) Anderson, M. T.; Poeppelmeier, K. R. *Chem. Mater.* **1991**, *3*, 476.
(12) Anderson, M. T.; Poeppelmeier, K. R. *J. Solid State Chem.* **1993**, *102*, 164.
(13) Izumi, F. *The Rietveld Method*; Oxford University Press: Oxford, U.K., 1993; Chapter 13.

10.1021/cm980217g CCC: $15.00
Published on Web 08/15/1998

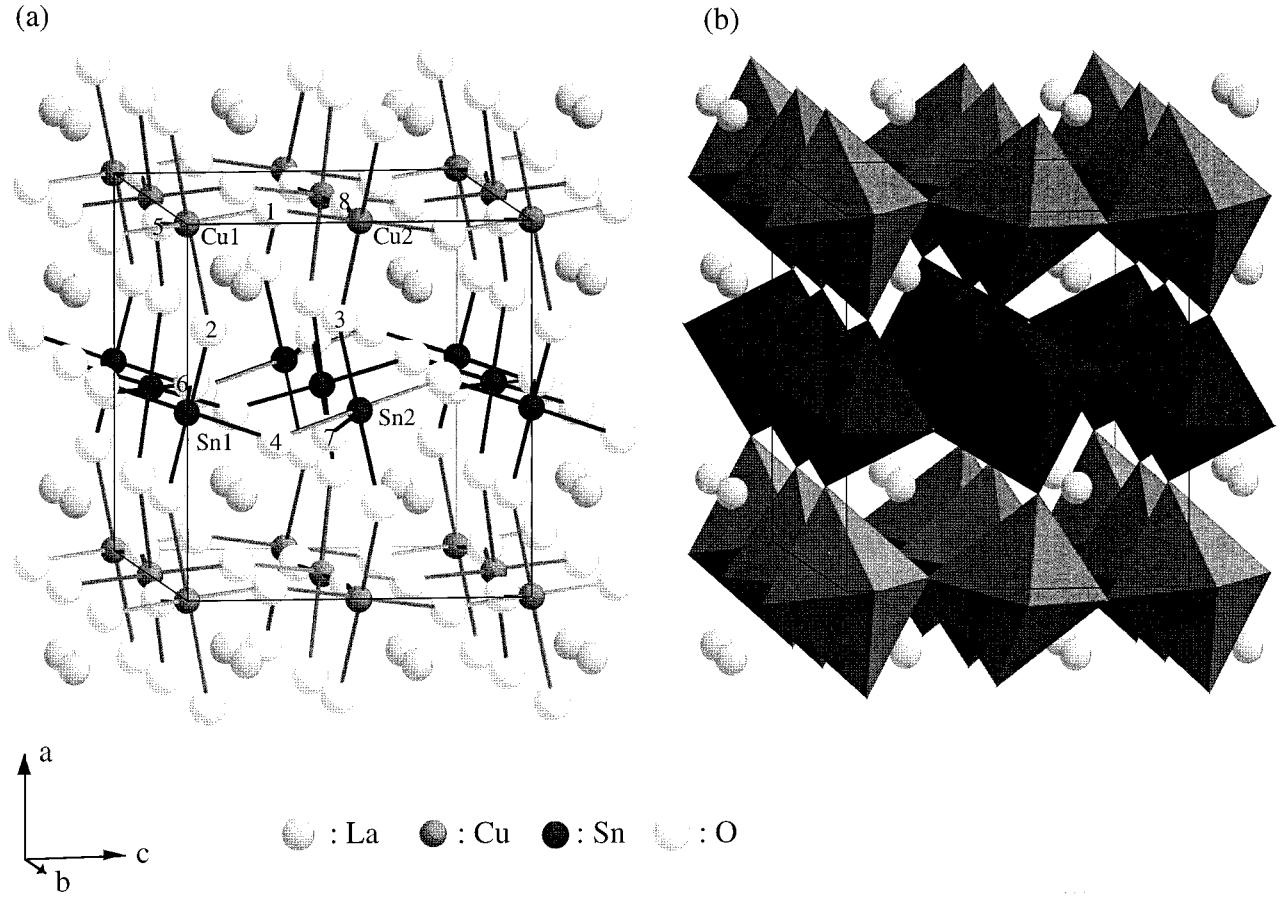

Figure 1. Crystal structure of La_2CuSnO_6.

mixtures of Ln_2CuO_4, $Ln_2Sn_2O_7$ (pyrochlore), and CuO. These mixtures were treated at high pressure and high temperature for 30 min in a conventional cubic-anvil type high-pressure apparatus. The conditions to obtain the most homogeneous samples were 6 GPa and 1000 °C for Ln = Pr and 6 GPa and 1200 °C for Ln = Nd. Considerable amounts of Sm_2CuO_4 and $Sm_2Sn_2O_7$ remained in the Ln = Sm sample even after the treatment at 8 GPa and 1200 °C. Higher pressure and/or temperature appears to be necessary to obtain a single phase sample of Sm_2CuSnO_6. Samples of La_2CuMO_6 (M = Ti, Ir, and Zr) were prepared from the mixtures of La_2O_3, CuO, and MO_2 in air at 1000 °C. Single phase samples were obtained for M = Ti and Ir in the same form as that reported before,[8−10] whereas a mixture of La_2CuO_4, $La_2Zr_2O_7$ (pyrochlore), and CuO was obtained for La_2CuZrO_6. These were treated at high pressure and high temperature, as mentioned later, and examined as well.

Structural Analysis. Powder X-ray diffraction data were collected for each sample with a Rigaku RINT 2000 difractometer equipped with monochromator (Cu Kα radiation, 30 kV, 200 mA). Si powder (NIST-640b) was used to calibrate the goniometer. Data were collected from 20 to 120° with a step of 0.02°. Lattice parameters and the atomic positions were refined by a Rietveld technique using Rietan software.[14] Isotropic atomic displacement parameter *B* was fixed and not refined. Only lattice parameters were refined for Sm_2CuSnO_6 because of the mixing of considerable amounts of Sm_2CuO_4, $Sm_2Sn_2O_7$, and some unknown impurities.

Magnetic Measurements. A SQUID magnetometer (Quantum Design MPMS2) was used to measure the temperature and field dependence of the magnetization. For the temperature dependence, measurements were done on heating in a fixed field after zero-field cooling (ZFC) and cooling in the same fixed field (FC). The magnetization curve at a fixed temperature up to 9×10^4 Oe was measured after zero-field cooling by means of an extraction method using Quantum Design PPMS susceptometer.

(14) Endoh, Y.; Matsuda, M.; Yamada, K.; Kakurai, K.; Hidaka, Y.; Shirane, G.; Birgeneau, R. *J. Phys. Rev.* **1989**, *B40*, 7023.

Results and Discussion

Structure of Ln_2CuSnO_6. Figure 2 shows the results of Rietveld analyses on powder X-ray diffraction (XED) patterns of the La_2CuSnO_6, Pr_2CuSnO_6, and Nd_2CuSnO_6 samples. The analyses were performed on the basis of the same space groupe ($P2_1/m$) as determined by Anderson et al.[11] The observed, calculated, and difference patterns as well as the allowed reflections are displayed in the figure. Data were analyzed assuming the presence of $Ln_2Sn_2O_7$. The estimated mass fractions were 2.40, 2.72, and 3.43%, respectively. Crystallographic data and the reliability factors are summarized in Table 1. As shown in Figure 3, lattice constants *a*, *b*, and *c* decreased with decreasing lanthanide ionic radius (R_{Ln}), while β increased. The refined atomic positions are presented in Table 2. Cu−O bond lengths are calculated and listed in Table 3. Those in the CuO_2 sheet are plotted against R_{Ln} in Figure 4 with closed circles. Plotted with open circles for Ln = La are those estimated from the neutron diffraction data.[11] The Cu1−O5 bonds tended to decrease with decreasing ionic radius (R_{Ln}). However, contrary to expectation, Cu2−O8 bonds expanded slightly, and the other two bonds did not significantly change. This phenomenon can be explained by considering the Cu−O−Cu bond angles which are summarized in Table 3 and Figure 5. The average Cu−O−Cu bond

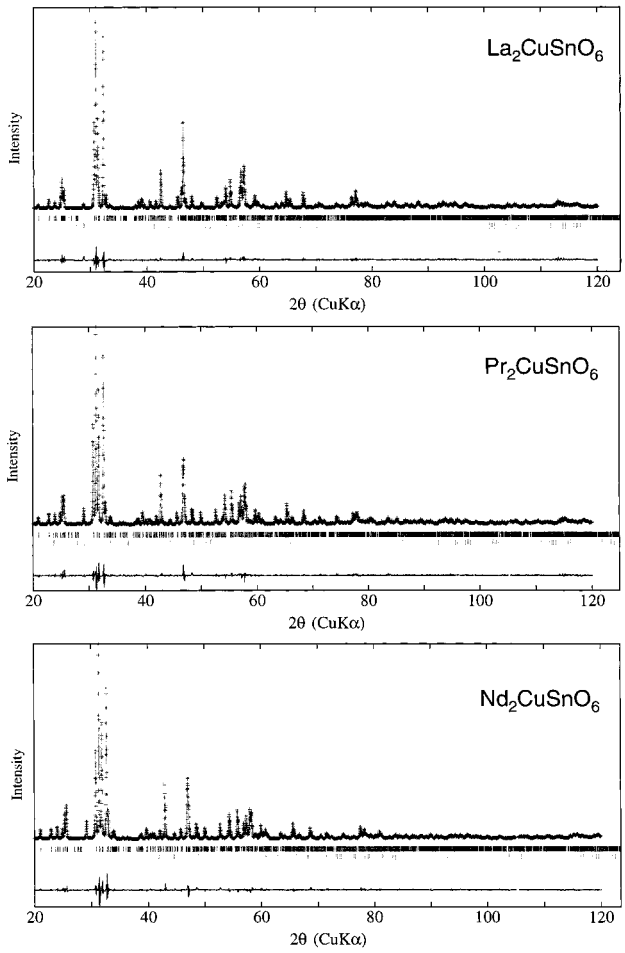

Figure 2. Observed (+), calculated (solid line), and difference (below) XRD patterns of La_2CuSnO_6, Pr_2CuSnO_6, and Nd_2CuSnO_6. The upper set of tic marks indicates the calculated peak positions for Ln_2CuSnO_6, and the lower set represents those of $Ln_2Sn_2O_7$.

Table 1. Crystallographic Data of Ln_2CuSnO_6 (Ln = La, Pr, and Nd)

formula	La_2CuSnO_6	Pr_2CuSnO_6	Nd_2CuSnO_6
space group	$P2_1/m$	$P2_1/m$	$P2_1/m$
a (Å)	8.5032(1)	8.4412(1)	8.4100(2)
b (Å)	7.8109(1)	7.7395(1)	7.7132(2)
c (Å)	7.8131(1)	7.7625(1)	7.7400(2)
β (deg)	91.143(1)	91.716(1)	92.011(1)
V (Å^3)	518.824	506.908	501.774
radiation	Cu Kα	Cu Kα	Cu Kα
monochromator	graphite	graphite	graphite
Z	4	4	4
2θ range (deg)	20−120	20−120	20−120
2θ step-scan increasement	0.02	0.02	0.02
R_{wp} (%)	4.49	4.89	4.54
R_p (%)	3.40	3.70	3.40
goodness-of fit	1.0795	1.1828	1.2004

angle becomes smaller and the deviation from 180° larger with decreasing R_{Ln}. The decrease in lattice constants results in an increased buckling of the CuO_2 plane.

Ln_2CuSnO_6 consists of three kinds of 2D layers, CuO_2, SnO_2, and LaO layers. The ideal size of a CuO_2 layer is between those of the SnO_2 and the LaO layers because Sn^{4+} has an ionic radius larger than Cu^{2+} and a LaO layer has the rock salt configuration. The mismatching is compromised by tilting, rather than elastic deformation, of the CuO_6 and SnO_6 octahedra. This is the reason for the heavy buckling of the CuO_2 layers. The

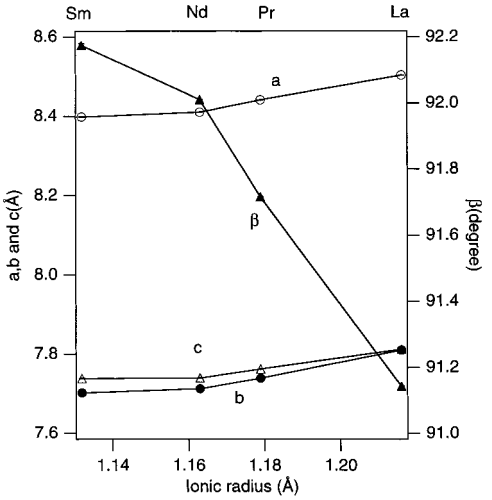

Figure 3. Lattice parameters of La_2CuSnO_6, Pr_2CuSnO_6, Nd_2CuSnO_6, and Sm_2CuSnO_6 as a function of the ionic radius of the lanthanide ion (R_{Ln}).

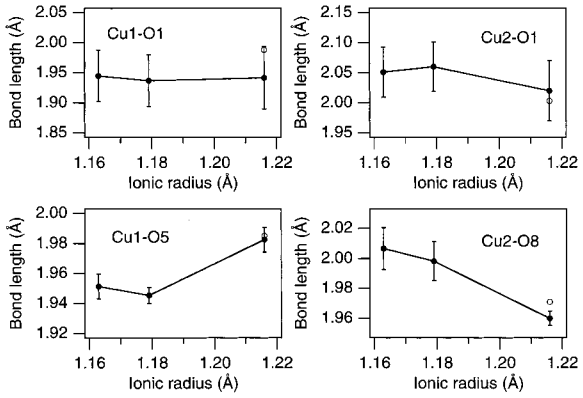

Figure 4. In-plane Cu−O bond length of Ln_2CuSnO_6 (Ln = La, Pr, and Nd) as a function of the ionic radius of the lanthanides ion (R_{Ln}).

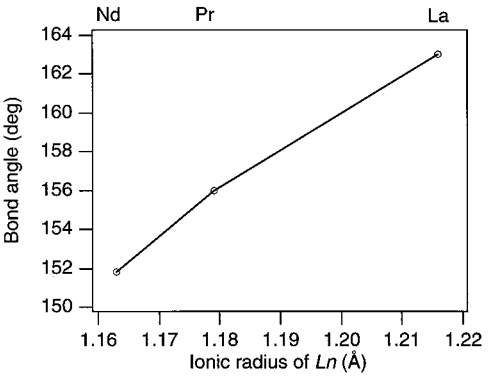

Figure 5. Average Cu−O−Cu bond angle in a CuO_2 plane as a function of the ionic radius of the lanthanide ion (R_{Ln}).

replacement of La by Pr and Nd results in a larger mismatch between the CuO_2 and LnO layers and a more serious buckling of the CuO_2.

Magnetic Property of Ln_2CuSnO_6. Figure 6a shows the temperature dependence of magnetization divided by field (M/H) of La_2CuSnO_6 measured in an external magnetic field of 100 Oe. When the sample is cooled in zero field, the magnetization measured on heating exhibits a maximum centered at 215 K. In contrast, on field-cooling the magnetization approaches

Table 2. Atomic Positions for Ln_2CuSnO_6 (Ln = La, Pr, and Nd)

atom	site	*x*	*y*	*z*	*B*
		La_2CuSnO_6			
La1	2e	0.2110(9)	0.25	0.276(1)	0.400
La2	2e	0.199(1)	0.25	0.772(1)	0.400
La3	2e	0.7588(8)	0.25	0.786(1)	0.400
La4	2e	0.7704(8)	0.25	0.275(1)	0.400
Cu1	2a	0	0	0	0.500
Cu2	2c	0	0	0.5	0.500
Sn1	2b	0.5	0	0	0.600
Sn2	2d	0.5	0	0.5	0.600
O1	4f	0.029(4)	−0.027(5)	0.245(7)	1.000
O2	4f	0.272(4)	−0.053(6)	−0.049(5)	1.000
O3	4f	0.262(4)	0.061(6)	0.546(5)	1.000
O4	4f	0.426(3)	0.037(4)	0.244(4)	1.000
O5	2e	0.029(6)	0.25	0.030(8)	1.000
O6	2e	0.455(5)	0.25	−0.067(7)	1.000
O7	2e	0.594(5)	0.25	0.531(7)	1.000
O8	2e	−0.007(7)	0.25	0.479(8)	1.000
		Pr_2CuSnO_6			
Pr1	2e	0.2069(0)	0.25	0.281(1)	0.400
Pr2	2e	0.1950(9)	0.25	0.772(1)	0.400
Pr3	2e	0.7557(7)	0.25	0.791(1)	0.400
Pr4	2e	0.7669(8)	0.25	0.280(1)	0.400
Cu1	2a	0	0	0	0.500
Cu2	2c	0	0	0.5	0.500
Sn1	2b	0.5	0	0	0.400
Sn2	2d	0.5	0	0.5	0.400
O1	4f	0.040(4)	−0.043(4)	0.243(5)	1.000
O2	4f	0.251(3)	−0.032(6)	−0.071(5)	1.000
O3	4f	0.271(5)	0.060(5)	0.558(5)	1.000
O4	4f	0.379(5)	0.032(5)	0.229(5)	1.000
O5	2e	0.020(6)	0.25	0.014(8)	1.000
O6	2e	0.466(5)	0.25	−0.086(7)	1.000
O7	2e	0.567(5)	0.25	0.533(8)	1.000
O8	2e	−0.002(6)	0.25	0.435(7)	1.000
		Nd_2CuSnO_6			
Nd1	2e	0.2074(6)	0.25	0.282(1)	0.400
Nd2	2e	0.1918(7)	0.25	0.771(1)	0.400
Nd3	2e	0.7541(6)	0.25	0.7954(9)	0.400
Nd4	2e	0.7672(7)	0.25	0.2828(9)	0.400
Cu1	2a	0	0	0	0.500
Cu2	2c	0	0	0.5	0.500
Sn1	2b	0.5	0	0	0.400
Sn2	2d	0.5	0	0.5	0.400
O1	4f	0.039(4)	−0.048(4)	0.244(6)	1.000
O2	4f	0.256(3)	−0.041(6)	−0.065(5)	1.000
O3	4f	0.267(4)	0.053(5)	0.559(5)	1.000
O4	4f	0.398(4)	0.036(4)	0.233(5)	1.000
O5	2e	0.023(5)	0.25	0.029(8)	1.000
O6	2e	0.458(5)	0.2500	0−0.092(7)	1.000
O7	2e	0.566(5)	0.25	0.525(8)	1.000
O8	2e	−0.002(5)	0.25	0.428(7)	1.000

Table 3. Selected Bond Lengths (Å) and Angles (deg) for Ln_2CuSnO_6 (Ln = La, Pr, and Nd)

	La_2CuSnO_6	Pr_2CuSnO_6	Nd_2CuSnO_6
in-plane			
Cu1−O1	1.94(5)	1.93(4)	1.94(4)
Cu1−O5	1.982(8)	1.945(5)	1.951(8)
Cu2−O1	2.02(5)	2.06(4)	2.05(4)
Cu2−O8	1.960(5)	1.99(1)	2.00(1)
out-of-plane			
Cu1−O2	2.39(3)	2.22(3)	2.25(3)
Cu2−O3	2.30(3)	2.37(4)	2.31(6)
Cu1−O5−Cu1	160.1	168.1	162.4
Cu2−O8−Cu2	170.1	151.1	147.9
Cu1−O1−Cu2	160.8	152.3	151.2
av bond angle	163.0	156.0	151.8

saturation at low temperature. The ferromagnetic hysteresis can also be seen clearly in the *M*−*H* curve, as shown in Figure 6b. La^{3+} and Sn^{4+} are both nonmagnetic, so this behavior directly demonstrates the antiferromagnetic nature of the CuO_2 lattice accompanied by a spin-canted weak ferromagnetism, as reported before.[12] The saturation magnetization measured on cooling to 5 K corresponds to a ferromagnetic moment of 6.4×10^{-3} μ_B/Cu. If the Cu^{2+} ions are assumed to have an atomic moment of 0.5 μ_B as in Nd_2CuO_4,[14] the canting angle is calculated to be 0.37°. This is considerably larger than that of Y_2CuO_4, which has the T′ structure (0.05°),[15] possibly reflecting larger buckling of the CuO_2 layer in the present compound.

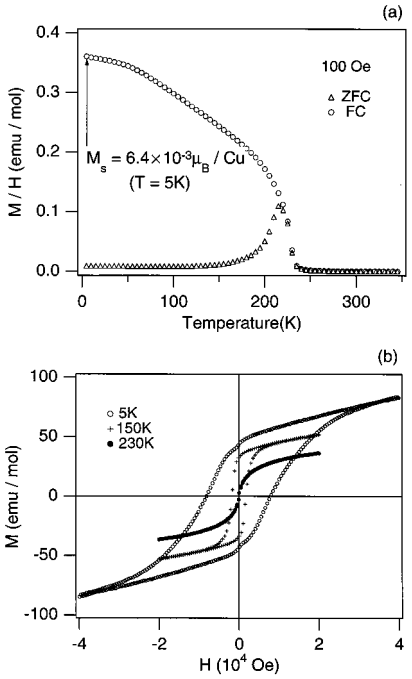

Figure 6. Temperature dependence of the magnetic susceptibility of La_2CuSnO_6 measured in a applied field of 100 Oe (a). (b) Magnetization curves measured at 5, 150, and 230 K.

Magnetism of Pr_2CuSnO_6 and Nd_2CuSnO_6. Figure 7a shows the *M*/*H* data of Pr_2CuSnO_6 measured at 100 Oe. The data are almost identical to that of La_2CuSnO_6 above 100 K but are significantly different at lower temperatures. Because Pr^{3+} has an atomic moment, the magnetization should reflect contributions from the Cu^{2+} and Pr^{3+} ions. The solid line in Figure 7a represents the estimated total *M*/*H* as a sum of the susceptibility of the paramagnetic Pr^{3+} ion and the zero-field cooled *M*/*H* data for La_2CuSnO_6. The former was calculated on the basis of the theoretical value of $\mu_J = g\mu_B[J(J+1)] = 3.58$ μ_B. For comparison, $\mu_J = 3.62$ μ_B for Nd^{3+} and 0.845 μ_B for Sm^{3+}. The observed values at low temperatures below 10 K are considerably larger than the estimation. This indicates that Pr in this compound also has some magnetic ordering. In the *M*/*H* data measured in a lower field of 5 Oe, as shown in Figure 7b, an antiferromagnetic-like cusp can be seen at 35 K. This is close to the ordering temperature of Sm and Gd moments of Sm_2CuO_4 (6 K) and Gd_2CuO_4 (7 K).[16]

Figure 8 shows the *M*/*H* data of Nd_2CuSnO_6 measured at 100 Oe on heating and cooling. There are three distinct features: a lack of the clear difference between

(15) Okuda, H.; Takano, M.; Takeda, Y. *Phys. Rev.* **1990**, *B42*, 6813.
(16) Johnston, D. C. *Handbook of Magnetic Materials*; Elsevier Science: Amsterdam, 1997; Vol. 10, Chapter 1.

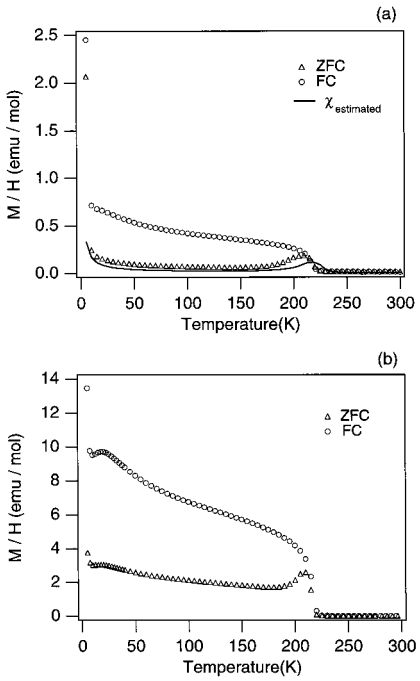

Figure 7. Temperature dependence of the magnetic susceptibility of Pr_2CuSnO_6 measured at 100 (a) and 5 Oe (b).

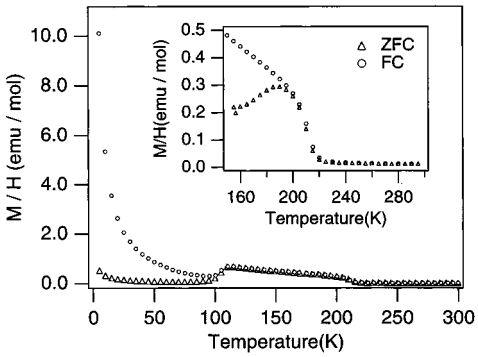

Figure 8. Temperature dependence of the magnetic susceptibility of Nd_2CuSnO_6 measured at 100 Oe. Inset represents the data collected in the temperature range of 150−300 K.

the data collected on heating and cooling below 200 K, an antiferromagnetic-like cusp at 110 K, and a large magnetization at lower temperatures. To investigate the reason for the absence of the difference between the ZFC and FC data below 200 K, the sample was cooled in zero field and the magnetic field was applied at 150 K before measuring the susceptibility on heating. The result is shown in the inset to Figure 8. The ferromagnetic hysteresis, owing to the weak ferromagnetism of the Cu^{2+} ions, reappeared. This indicates that Cu spins exhibit essentially the same spin-canted weak ferromagnetism as was observed in La_2CuSnO_6. T_N is plotted as a function of the ionic radius of Ln in Figure 9. The observed T_N range of 200−235 K is similar to that of Nd_2CuO_4, 255 K.[14] This suggests that the magnitude of antiferromagnetic interaction (J) is approximately the same; both are magnetically two-dimensional, and the conduction bands are of $d_{x^2-y^2}$ parentage. The decrease in T_N with the smaller Ln ion can be attributed to the decrease of J between Cu spins as a result of the increased buckling of the Cu−O−Cu bond in the CuO_2 planes. If the unpaired electron is in the d_{z^2} orbital, the antiferromagnetic interaction is

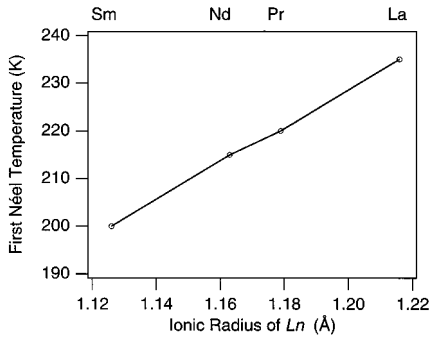

Figure 9. Néel temperature of Cu sublattice of Ln_2CuSnO_6 (Ln = La, Pr, Nd, and Sm) as a function of R_{Ln}.

mediated through the long Cu−O−Sn−O−Cu bonds and should be much weaker than the superexchange through the Cu−O−Cu bonds in a CuO_2 plane. Moreover, in this case, the system should be one-dimensional approximately. For these two reasons, T_N should be much lower. The assumption that the conduction bands are of $d_{x^2-y^2}$ parentage is consistent with a recent band calculation;[17] nonetheless the shrinkage of the out-of-plane dimension with hole-doping observed in La_2CuSnO_6 cannot be explained easily.

The nonlinearlity at 150 K corresponding to the weak ferromagnetism of Cu ions can be seen in the magnetization curve shown in Figure 10. However, the spontaneous moment of 0.65 μ_B/mol at 2 K is too large to be assigned to the Cu sublattice only. Therefore, it is reasonable to conclude that Nd sublattice orders in a canted antiferromagnetic spin structure as well. We assume that both ferromagnetic moments order antiferromagnetically at 110 K. There are two Néel temperatures in Nd_2CuSnO_6. The first one (T_{N1}) is the antiferromagnetic transition temperature of the Cu sublattice. The ordering is faintly ferromagnetic, and clear hysteresis is observed between the ZFC and FC data below the transition temperature when the data are collected in the temperature range above the second transition temperature (T_{N2}). The Nd sublattice orders antiferromagnetically, and the ordering is weakly ferromagnetically also because of spin canting. Therefore, the susceptibility data show clear hysteresis below T_{N2}. At T_{N2}, both ferromagnetic moments (on the Cu and Nd sublattices) order antiferromagnetically. T_{N2} was also observed in Pr_2CuSnO_6 and Sm_2CuSnO_6, as shown in Figure 11. However, why only Nd_2CuSnO_6 has an anomalously high T_{N2} is not clear. The magnetic moment of Nd^{3+} is close to that of Pr^{3+}, whereas Sm^{3+} is only about 20% of their values. Nonetheless Nd_2CuSnO_6 has a T_{N2} at 110 K, and the others are below 40 K.

Another possible explanation is to assume the occurrence of a spin−flop transition at 110 K. Suppose, for example, the spin axis changes from an in-plane axis to out-of-plane axis or vice versa. If the canting angle is smaller in the low-temperature phase, the weak ferromagnetic moment will drop as temperature decreases through the phase boundary. If the anisotropy of the weak-ferromagnetic moment is larger for the low-temperature phase, the difference between the FC and

(17) Novikov, D. J.; Freeam, A. J.; Poeppelmeier, K. R.; Zhukov, V. P. *Physica* **1995**, *C252*, 7.

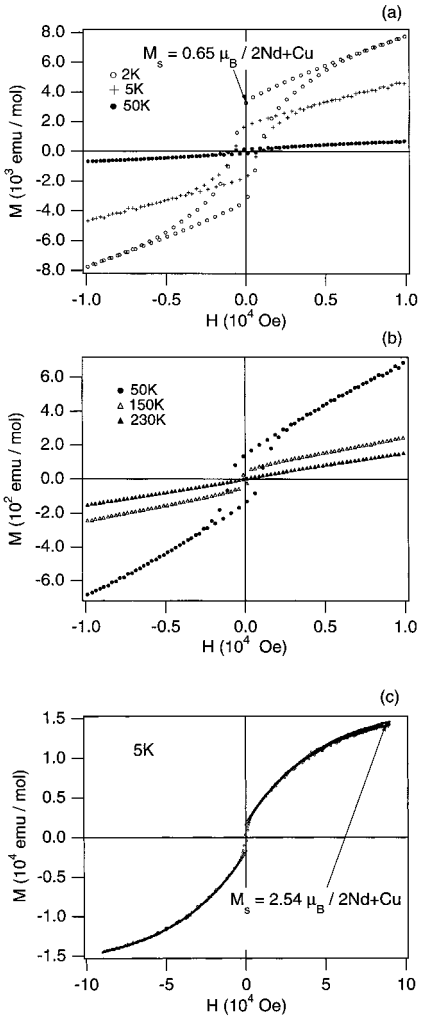

Figure 10. Magnetization curve of Nd_2CuSnO_6 measured at 2, 5, and 50 K (a) and 50, 150, and 230 K (b). (c) Data collected by means of an extraction method at 5 K.

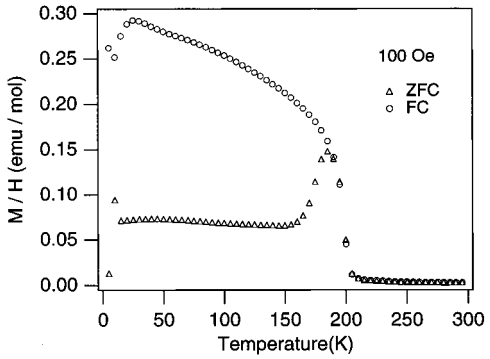

Figure 11. Temperature dependence of the magnetic susceptibility of Sm_2CuSnO_6 measured at 100 Oe.

ZFC data will be enhanced for the low-temperature phase.

Hole Doping of Nd_2CuSnO_6. Hole doping of Nd_2CuSnO_6 was carried out by substituting Ca^{2+} for Nd^{3+}. The sample was synthesized from a mixture of Nd_2CuSnO_6, Ca_2CuO_3, and SnO_2 at the same conditions used to prepare the pure sample. A 1 wt % amount of $KClO_4$ was added to the sample to generate an oxidizing atmosphere. Although a high-pressure−high-temperature treatment was repeated twice, a considerable amount of impurity phases remained in the final product. The lattice constants of $Nd_{1.9}Ca_{0.1}CuSnO_6$ were refined and are compared with those of the pure sample in Table 4. All the axes decreased in this case.

Table 4. Lattice Constants of Nd_2CuSnO_6 and $Nd_{1.9}Ca_{0.1}CuSnO_6$

	Nd_2CuSnO_6	$Nd_{1.9}Ca_{0.1}CuSnO_6$
a (Å)	8.4100(2)	8.3984(8)
b (Å)	7.7132(2)	7.7025(7)
c (Å)	7.7400(2)	7.7385(7)
β (deg)	92.011(1)	92.173(5)

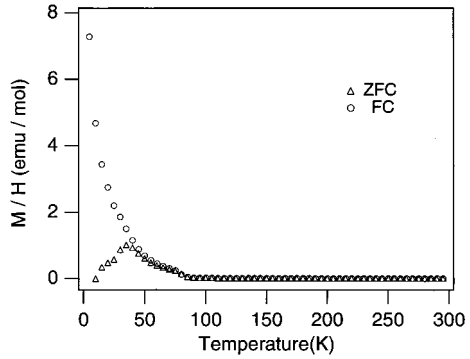

Figure 12. Temperature dependence of the magnetic susceptibility of $Nd_{1.9}Ca_{0.1}CuSnO_6$ measured at 100 Oe.

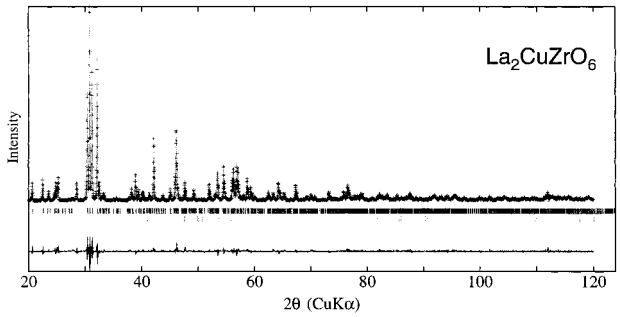

Figure 13. Observed (+), calculated (solid line), and difference (below) XRD patterns of La_2CuZrO_6. The upper set of tic marks indicates the calculated peak positions for La_2CuZrO_6, and the lower set represents those of $La_2Zr_2O_7$.

Table 5. Crystallographic Data of La_2CuZrO_6

formula	La_2CuZrO_6	monochromator	graphite
space group	$P2_1/m$	*Z*	4
a (Å)	8.5683(1)	2θ range (deg)	20−120
b (Å)	7.8597(1)	2θ step-scan increasement	0.02
c (Å)	7.8557(1)	R_{wp} (%)	5.95
β (deg)	91.512(1)	R_p (%)	4.43
V (Å^3)	528.934	goodness-of fit	1.4424
radiation	Cu Kα		

Figure 12 shows the *M*/*H* data of $Nd_{1.9}Ca_{0.1}CuSnO_6$. The Néel temperature decreased with doping as was the case with La_2CuSnO_6 and high T_c superconductors. Yet, similar to La_2CuSnO_6, no superconducting transition was observed.

La_2CuZrO_6. La_2CuMO_6 (M = Ti, Ir, Zr) were treated at high pressure and high temperature to look for a new variation of layered double perovskite. La_2CuTiO_6 and La_2CuIrO_6 did not change their structures after treatment at 8 GPa and 1200 °C. Peaks corresponding to a new phase were found in the XRD pattern of La_2CuZrO_6, while considerable amounts of La_2CuO_4 and $La_2Zr_2O_7$ remained. An almost single phase sample of La_2CuZrO_6 was synthesized directly from a mixture of La_2O_3, CuO, and ZrO_2 at 6 GPa and 1100 °C. The XRD

Table 6. Atomic Positions for La_2CuZrO_6

atom	site	*x*	*y*	*z*	*B*
La1	2e	0.206(1)	0.25	0.279(2)	0.400
La2	2e	0.197(1)	0.25	0.774(2)	0.400
La3	2e	0.7610(9)	0.25	0.787(2)	0.400
La4	2e	0.772(1)	0.25	0.279(2)	0.400
Cu1	2a	0	0	0	0.500
Cu2	2c	0	0	0.5	0.500
Zr1	2b	0.5	0	0	0.600
Zr2	2d	0.5	0	0.5	0.600
O1	4f	0.050(3)	−0.026(7)	0.247(6)	1.000
O2	4f	0.267(3)	−0.032(7)	−0.072(6)	1.000
O3	4f	0.266(5)	0.037(8)	0.574(6)	1.000
O4	4f	0.422(4)	0.049(5)	0.248(5)	1.000
O5	2e	0.019(7)	0.25	0.015(9)	1.000
O6	2e	0.458(6)	0.25	−0.075(8)	1.000
O7	2e	0.572(6)	0.25	0.541(9)	1.000
O8	2e	−0.005(8)	0.25	0.462(9)	1.000

pattern shown in Figure 13 is that expected of the layered double perovskite structure. A small amount of $La_2Zr_2O_7$, the estimated mass fraction being 3.26%, was present. Crystal data and reliability factors are summarized in Table 5. The refined atomic positions are presented in Table 6. The calculated Cu−O bond lengths and Cu−O−Cu bond angles are listed in Table 7 together with those of La_2CuSnO_6. The in-plane bond lengths expanded slightly, and the average Cu−O−Cu bond angle decreased again. The replacement of Zr for Sn induced a larger mismatch between the CuO_2 and ZrO_2 layers and, as a result, the CuO_2 layer buckled even more.

Conclusions

Ln_2CuSnO_6 (Ln = Pr, Nd, and Sm) were stabilized in the same layered double perovskite structure as La_2CuSnO_6 at high pressures of 6−8 GPa and high temperatures of 1000−1200 °C. Replacement of La by smaller lanthanides increased the buckling in the CuO_2 layers. As a result, the antiferromagnetic transition temperature of the Cu sublattice decreased monotonically. The magnetic moment of Nd ion was found to exhibit weak ferromagnetism as well. La_2CuZrO_6, a new member of layered double perovskite with a tetravalent cation, was found at 6 GPa and 1100 °C. Replacement of Sn by larger Zr also caused the buckling of the CuO_2 layer to increase.

Table 7. Selected Bond Lengths (Å) and Angles (deg) for La_2CuSnO_6 and La_2CuZrO_6

	La_2CuSnO_6	La_2CuZrO_6
Bond Length		
in-plane		
Cu1−O1	1.94(5)	1.99(5)
Cu1−O5	1.982(8)	1.975(6)
Cu2−O1	2.02(5)	2.06(5)
Cu2−O8	1.960(5)	1.99(1)
out-of-plane		
Cu1−O2	2.39(3)	2.38(3)
Cu2−O3	2.30(3)	2.35(4)
Bond Angle		
Cu1−O5−Cu1	160.1	168.4
Cu2−O8−Cu2	170.1	163.0
Cu1−O1−Cu2	160.8	152.8
average bond angle	163.0	159.2

Acknowledgment. The authors express their thanks to Prof. K. R. Poeppelmeier for useful discussion as a Japan Society for the Promotion of Science (JSPS) fellow. This work was partly supported by a Grant-in Aid for Scientific Research on Priority Areas, “Anomalous metallic state near the Mott transition”, of the Ministry of Education, Science and Culture, Japan, and CREST (Core Research for Evolutional Science and Technology) of the Japan Science and Technology Corp. (JST).

CM980217G